Title page information

Title:

Trends in anthropogenic CO_2 in water masses of the Subtropical North Atlantic Ocean.

Authors:

Elisa F. Guallart[a,*], Ute Schuster[b,1*], Noelia M. Fajar[c], Ollie Legge[b], Peter Brown[b,d], Carles Pelejero[a,e], Marie-Jose Messias[b,1*], Eva Calvo[a], Andrew Watson[b,1*], Aida F. Ríos[c] and Fiz F. Pérez[c].

Address:

[a]Institut de Ciències del Mar, CSIC, Pg. Marítim de la Barceloneta 37-49, E-08003, Barcelona, Spain.

[b]Centre for Ocean and Atmospheric Science, School of Environmental Sciences, University of East Anglia, Norwich, NR4 7TJ, UK.

[c]Instituto de Investigacións Mariñas, CSIC, Eduardo Cabello 6, E-36208, Vigo, Spain.

[d] British Antarctic Survey, Cambridge, CB3 0ET, UK

[e]Institució Catalana de Recerca i Estudis Avançats, Passeig Lluís Companys 23, E-08010, Barcelona, Spain.

[*]Corresponding author: Elisa F. Guallart

Tel: +34 93 230 9500; Fax: + 34 93 230 95 55

E–mail addresses: efernandez@icm.csic.es (E.F. Guallart), u.schuster@exeter.ac.uk (U. Schuster), nfajar@iim.csic.es (NM. Fajar), o.legge@uea.ac.uk (O. Legge), P.J.Brown@uea.ac.uk (P. Brown), carles.pelejero@icrea.cat (C. Pelejero), m.messias@exeter.ac.uk (MJ. Messias), , ecalvo@icm.csic.es (E. Calvo), andrew.watson@exeter.ac.uk (A. Watson), aida@iim.csic.es (A.F. Ríos), fiz.perez@iim.csic.es (F.F. Pérez).

[1] Present address: College of Life and Environmental Sciences, University of Exeter, Exeter, EX4 4PS, UK.

Abstract

The variability in the storage of the oceanic anthropogenic CO_2 (C_{ant}) on decadal timescale is evaluated within the main water masses of the Subtropical North Atlantic along 24.5°N. To this aim, CO_2 measurements on five cruises of the A05 section are used to assess the changes in C_{ant} between 1992 and 2011 in the presence of variability in circulation, using four methodological procedures (ΔC^*, TrOCA, φC_T^0, TTD). We find good agreement between the results obtained using chlorofluorocarbons and CO_2 measurements. The overall C_{ant} distribution showed higher concentrations and greater decadal storage rates in the upper layers with both values decreasing towards the bottom. The central water masses presented the greatest C_{ant} enrichment, with their upper limb showing a mean yearly accumulation of about ~1 $\mu mol \cdot kg^{-1} \cdot yr^{-1}$ and the lower limb showing, on average, half of that value. The much lower mean storage rates found in intermediate and deep layers (all of them being lesser than ~ 0.25 $\mu mol \cdot kg^{-1} \cdot yr^{-1}$) became more relevant when longitudinal differences in the C_{ant} accumulation were considered. In particular, west of 70°W the ventilation by the Labrador Sea Water created a noticeable accumulation rate up to ~0.5 $\mu mol \cdot kg^{-1} \cdot yr^{-1}$ between 1000 and 2500 dbar. If a transient stationary state of the C_{ant} distributions is considered, significant bi-decadal trends in the C_{ant} storage rates of the deepest North Atlantic waters are detected, in agreement with recent estimations. In the upper layers, our results suggest that, over the course of the last two decades, C_{ant} was absorbed more intensely in the western side of the North Atlantic SubTropical Gyre, although C_{ant} concentrations were greater in the east. These findings are in accordance with data reported in fixed Time Series Stations.

Keywords:

Anthropogenic CO_2; C_{ant} storage rates; Decadal variability; C_{ant} estimation; Steady State; Water masses.

Atlantic Ocean; Subtropical North Atlantic Gyre; DeepWestern Boundary Current.

Abbreviations:

C_{ant}	Anthropogenic CO_2.
$[C_{ant}]$	Mean C_{ant} concentrations, in µmol·kg^{-1}.
$[C_{ant}^{\varphi C_T^0}]$	Mean C_{ant} values estimated by the φC_T^0 method, in µmol·kg^{-1}.
$[C_{ant}^{TrOCA}]$	Mean C_{ant} values estimated by the TrOCA method, in µmol·kg^{-1}.
$[C_{ant}^{\Delta C^*}]$	Mean C_{ant} values estimated by the ΔC^* method, in µmol·kg^{-1}.
$[C_{ant}^{TTD}]$	Mean C_{ant} values estimated by the TTD method, in µmol·kg^{-1}.
DT(φC_T^0)	Decadal Trend ± uncertainty in C_{ant} accumulation by the φC_T^0 method, in µmol·kg^{-1} yr^{-1}.
DT(TrOCA)	Decadal Trend ± uncertainty in C_{ant} accumulation by the TrOCA method, in µmol·kg^{-1} yr^{-1}.
DT(ΔC^*)	Decadal Trend ± uncertainty in C_{ant} accumulation by the ΔC^* method, in µmol·kg^{-1} yr^{-1}.
DT(TTD)	Decadal Trend ± uncertainty in C_{ant} accumulation by the TTD method, in µmol·kg^{-1} yr^{-1}.
TSSR(φC_T^0)	Transient Stationary State rate ± uncertainty in C_{ant} accumulation by the φC_T^0 method, in µmol·kg^{-1} yr^{-1}.
TSSR(TrOCA)	Transient Stationary State rate ± uncertainty in C_{ant} accumulation by the TrOCA method, in µmol·kg^{-1} yr^{-1}.
TSSR(ΔC^*)	Transient Stationary State rate ± uncertainty in C_{ant} accumulation by the ΔC^* method, in µmol·kg^{-1} yr^{-1}.
TSSR(TTD)	Transient Stationary State rate ± uncertainty in C_{ant} accumulation by the TTD method, in µmol·kg^{-1} yr^{-1}.

1. Introduction

The ocean plays a major role as a sink for carbon dioxide (CO_2) released by humankind to the atmosphere, annually contributing to the removal of about one quarter of the total anthropogenic CO_2 (C_{ant}) atmospheric emissions (Khatiwala et al., 2013). The North Atlantic Ocean plays an important part absorbing and, especially, accumulating C_{ant} (Watson et al., 1995; Vázquez-Rodríguez et al., 2009a; Pérez et al., 2010a). It contains up to 25% of the oceanic $C_{ant,}$ although its surface represents only 13% of the global ocean (Sabine et al., 2004). Actually, despite its large C_{ant} storage rate, air-sea uptake in the North Atlantic is not predominantly anthropogenic, since the natural CO_2 uptake largely prevails over the anthropogenic perturbation in the North Atlantic Subpolar Gyre (NASPG) (Pérez et al., 2013). The C_{ant} entrance into the ocean interior takes place in the NASPG owing to deep convection, significantly contributing to the efficiency of the North Atlantic sink. This C_{ant} entrance is supported up to 65±13% due to lateral transports that carry C_{ant}-loaded subtropical waters to these northern latitudes through the upper limb of the Meridional Overturning Circulation (MOC) (Álvarez et al., 2003; Macdonald et al., 2003; Rosón et al., 2003; Pérez et al., 2013). At 24.5ºN, the MOC is responsible for almost 90% of the meridional heat flux (Johns et al., 2011) and it also transports up to 0.17-0.20 $PgC \cdot y^{-1}$ of C_{ant} (Macdonald et al., 2003; Rosón et al., 2003). Since the North Atlantic Subtropical Gyre (NASTG) has a prevailing role in the C_{ant} uptake from the atmosphere, the WOCE A05 hydrographic line situated at 24.5°N plays a relevant role in the evaluation and quantification of the C_{ant} build-up in the North Atlantic sink. It has been studied several times from high spatial resolution *in situ* CO_2 system measurements performed in 1992 (Rosón *et al.*, 2003), in 1998 (Macdonald *et al.*, 2003) and in 2004 (Brown et al., 2010). Two new recent occupations, in 2010 and 2011, add to this historical record.

Estimating the C_{ant} storage in the ocean is not simple because C_{ant} is a small perturbation (3% at the most) on the natural bulk of oceanic inorganic carbon (C_T). Since C_{ant} is not directly measured in the ocean, it has to be estimated based on indirect techniques from in-situ observations. Brewer (1978) and Chen and Millero (1979) presented the first C_{ant} calculations in the late 1970s, which attempted to separate the C_{ant} signal from the background CO_2 distribution by correcting the measured C_T for changes due to biological activity and by removing an estimate of the preindustrial preformed C_T. Several authors have tried to improve those first back-calculation methods (also called carbon-based), leading to a number of methodologies: ΔC^*(Gruber et al., 1996), ΔC_T^0 (Kortzinger et al., 1998), TrOCA (Touratier and Goyet, 2004; Touratier et al., 2007) and φC_T^0 (Vázquez-Rodríguez et al., 2009b). Overall, they rely on the general assumption that ocean circulation and the biological pump have operated in a steady state since the preindustrial time. In addition, some more recent conceptual approaches (Broecker and Peng, 1974; Thomas and Ittekkot, 2001; Haine and Hall, 2002) do not use C_T measurements and treat C_{ant} as a conservative tracer (i.e. a tracer that is not influenced by biological processes in the ocean), avoiding the uncertainties related to the biological correction of the back-calculation methodologies. Tracer distributions can be established by using the so-called TTD functions (Transient Time Distributions), that are mathematical expressions which serve to constrain the time elapsed since a water parcel was last in contact with the surface (Waugh et al., 2004; Waugh et al., 2006; Steinfeldt et al., 2009), to describe how the oceans circulation connects and transports C_{ant} from the surface to the ocean interior. Nevertheless, there is no clear consensus about the more appropriate method to estimate C_{ant} (Sabine and Tanhua, 2010). While some authors have reported C_{ant} estimations using only one method, ΔC^* (Macdonald et al., 2003; Rosón et al., 2003), TTD (Tanhua et al., 2008) or φC_T^0 (Pérez et al., 2010a; Ríos et al., 2012), other authors have decided running together two or more methods to compare the obtained results: TrOCA and φC_T^0 (Pérez et al., 2010b; Castaño-Carrera et al., 2012; Fajar et al., 2012), TrOCA, φC_T^0 and ΔC^*, (Flecha et al., 2012), ΔC^*, ΔC_T^0 and TrOCA (Lo Monaco et al., 2005) or ΔC^*, TrOCA, IPSL, TTD and φC_T^0 (Vázquez-Rodríguez et al., 2009b). Moreover, some authors suggest that a combination of approaches should be necessary to achieve a robust quantification of the ocean sink of C_{ant} (Khatiwala *et al.*, 2013).

The A05 repeat section cruises provide a valuable time series to better constrain the decadal variability of the North Atlantic C_{ant} storage from observational data. To this aim, the present work studies the C_{ant} changes between 1992 and 2011 along 24.5°N through four methodological procedures. Three back calculation methods (ΔC^* (Gruber et al., 1996), TrOCA (Touratier *et al.*, 2007) and φC_T^0 (Vázquez-Rodríguez et al., 2009b)) and a tracer based technique (TTD (Waugh *et al.*, 2006)) are used to quantify the temporal changes in the C_{ant} concentrations within six different water masses of the Subtropical North Atlantic. This study also faces possible longitudinal differences in the decadal C_{ant} storage rates and provides a general approximation of the results to a transient stationary state of oceanic C_{ant} accumulation.

2. Data

Five cruises of the A05 repeated section are used to study the temporal evolution of the C_{ant} storage in the Subtropical North Atlantic Ocean. Table 1 summarizes the information of interest relative to each one. The cruises carried out in 1992, 1998 and 2004 are referred as earlier cruises, with respect to the two most recent occupations in 2010 and 2011. All the cruises tracks are depicted in figure 1a: the 1992 occupation was carried out along 24.5°N, lying south of the following cruises at boundary regions and sampling the Florida Strait at 26°N. Subsequent occupations were set starting from 28°N next to the African shelf, joining the 24.5°N line at 24°W and angling northward near the opposite shelf to complete the line at 26.5°N, sampling the Florida Strait at 27°N. Among them, only the 2010 cruise crossed the Mid Atlantic Ridge (MAR) following the Kane Fracture Zone, thus slightly deviating from the common track.

2.1. Earlier cruises

The corresponding datasets are available on the CDIAC website (http://cdiac.ornl.gov/). The 1992 cruise was conducted under the frame of the WOCE Project. Procedures for CO_2 system parameters analysis and its adjustment are described in Rosón *et al.* (2003) and Guallart et al. (2013). The 1998 measurements are reported in Peltola et al. (2001) and Macdonald *et al.* (2003). Due to the lack of nutrient data to compute C_{ant}, nutrient gaps in positions where C_T and A_T were available were filled by interpolation using a multiparameter linear regression (MLR) technique (Velo et al., 2010). In 2004, the section was reoccupied within the framework of the CLIVAR Program. The analysis methodologies are described in Cunningham (2005) and Brown *et al.* (2010). The 2004 dataset used in this work is a combination between the data available at CDIAC and the Florida Strait measurements submitted to the British Oceanographic Data Center (http://www.bodc.ac.uk/). The A_T gaps in bottles where C_T was available were filled from interpolated normalized A_T ($NA_T = A_T \cdot 35$ /

salinity). The interpolation was done on NA_T data because it is less variable than A_T (Millero et al., 1998).

2.2. Recent cruises

In 2010, the C_T was measured by coulometry (Dickson et al., 2007) and A_T was determined by potentiometric titration (Dickson *et al.*, 2007) using a VINDTA system (Marianda, Kiel, Germany). Certified reference material (CRM, batch 97) supplied by Scripps Institution of Oceanography was analysed twice daily. Accuracy was calculated as ±2.9 $\mu mol \cdot kg^{-1}$ (n = 399) for C_T and ±1.9 $\mu mol \cdot kg^{-1}$ (n = 397) for A_T. After Secondary Quality Control (2ndQC) (Tanhua et al., 2010b) on C_T, A_T, nutrients and oxygen (O_2) data, O_2 and silicate were bias-adjusted (Table 1). The C_T and A_T data are further described in Schuster et al. (2013). The CFCs were measured at the LGMAC lab following Smethie *et al.* (2000) and Law *et al.* (1994). Nutrient gaps were filled as described above. In 2011, the last occupation of the A05 section was carried as part of the Circumnavigation Expedition MALASPINA 2010 (http://www.expedicionmalaspina.es/). The pH was measured spectrophotometrically (Clayton and Byrne, 1993) and A_T was determined potentiometrically by titration at endpoint detection (Mintrop et al., 2000). A_T gaps were filled as reported above. The C_T was calculated from A_T and pH using the dissociation constants of Mehrbach et al. (1973) refitted by Dickson and Millero (1987) using the CO_2sys program (Pierrot et al., 2006). Discrete C_T samples were taken in 11 stations and analysed for quality control at the IIM-CSIC laboratory by coulometric determination using a SOMMA system (Johnson et al., 1998). The internal consistency between calculated and measured C_T was estimated to be of 0.9 ± 3.5 $\mu mol \cdot kg^{-1}$ (n=22). No adjustments were needed after 2ndQC.

3. Methods

3.1. C_{ant} determinations

Three back-calculation methods (ΔC^*(Gruber et al., 1996), φC_T^0 (Vázquez-Rodríguez et al., 2009b) and TrOCA (Touratier and Goyet, 2004; Touratier et al., 2007)) and one tracer-based method (TTD (Waugh et al., 2006)) were selected to determine the C_{ant} distributions. The overall uncertainties in C_{ant} are ±9 $\mu mol \cdot kg^{-1}$, ±5.2 $\mu mol \cdot kg^{-1}$, ±6.25 $\mu mol \cdot kg^{-1}$ and ±6

$\mu mol \cdot kg^{-1}$ for ΔC^*, φC_T^0, TrOCA and TTD estimates, respectively. Further details on the specific assumptions of each of the four methodologies are provided in Appendix A, in the Supplementary information.

3.2. Averaging by regions and layers

The five A05 datasets were divided vertically in six density layers and longitudinally into five regions that are depicted in figure 1b, over the salinity distribution of the 2011 cruise. The water column was divided by identifying the main water masses representative of the Subtropical North Atlantic Ocean following (Talley et al., 2011): North Atlantic Central Waters (*NACW*), Antarctic Intermediate Water (*AAIW*), North Atlantic Deep Waters (*NADW*) and Antarctic Bottom Water (*AABW*). The subducted thermocline (*NACW*) was further split in two main cores: the upper (*uNACW*), including a warm and saline component related with the SubTropical Mode Water and the lower (*lNACW*), denser and fresher, related with the SubPolar Mode Waters (McCartney and Talley, 1982). The limit between the *AAIW* and the u*NADW* was also better constrained according to the TS properties. Thus, the three uppermost layers were delimited using σ_0 along the isopycnals $\sigma_0 = 26.7\ kg \cdot m^{-3}$, $\sigma_0 = 27.2$ and $\sigma_0 = 27.6\ kg \cdot m^{-3}$ (Fig.1b). The *uNACW* layer includes depths between ~150 - 450 dbar. Since the isopycnal is tilted up towards the east, it is far shallower on the eastern side of the section, until ~250 dbar. This layer shows the highest salinity values of the water column, within an average of 36.6. The *lNACW* layer is located between ~250 and ~850 dbar. The *AAIW* (from ~600 to ~1100 dbar) encompasses the oxygen minimum zone in the shallower levels of the layer. The slight eastward salinization at these depths comes from the MW influence, as it spreads through the layer below. The two *NADW* components were delimited according to a reference level of 2000 dbar (σ_2), along $\sigma_2 = 37\ kg \cdot m^{-3}$ (Fig.1b). The *uNADW* layer extends from ~1100 to ~2500 dbar. Its freshening close to the western margin is related to the Labrador Sea Water (LSW) spreading. The *lNADW* layer fills the eastern basin from ~2100 dbar to the ocean floor but extends to ~4500 dbar in the western basin. The *AABW* was delimited in the western basin along the isopycnal $\sigma_4 = 45.9\ kg \cdot m^{-3}$. In addition to the water masses classification, the section was zonally divided separating the eastern and western basins at 45°W, each side of the Mid-Atlantic Ridge. The division of the western basin was refined in order to better constrain, in terms of its circulation features, the temporal variability of C_{ant} distributions. The Florida Strait was identified as an independent region ranging from 80°W to 78°W. It was isolated from the main section due to its independent behaviour in terms of transports (Schmitz and Richardson, 1991; Macdonald et al., 2003; Rosón et al., 2003). The zone of deep ventilation by the Deep Western Boundary Current (DWBC), Region 1 (R1), was separated from the ocean interior at 70°W, isolating it from Region 2 (R2), where AABW fills a considerable volume of the deep ocean. Despite not showing *a priori* remarkable oceanographic particularities, the eastern basin was also halved at 30°W, differentiating Region 3 (R3) and Region 4 (R4) to isolate the relative maximum of salinity of Mediterranean Water (MW) that enters the section from the African Coast.

A total of 25 boxes (Fig. 1b) were obtained, and the temporal variability of the mean C_{ant} estimations within them was studied. Data above 150 dbar were removed to avoid seasonal biological effects, since conservative tracers do not vary seasonally in the subsurface (100-200m) (Vázquez-Rodríguez et al., 2012). Mean C_{ant} values ($[C_{ant}^{\varphi C_T^0}]$, $[C_{ant}^{TrOCA}]$, $[C_{ant}^{\Delta C^*}]$, $[C_{ant}^{TTD}]$, in $\mu mol \cdot kg^{-1}$) of the φC_T^0, TrOCA, ΔC^* and TTD estimates within each box were computed as the mean and standard deviation of the corresponding ensembles of 100 averages obtained through random perturbations of the φC_T^0, TrOCA, ΔC^* and TTD estimates in each box. The random perturbation of the data was done according to each method uncertainty. The values obtained are shown, for each cruise, in Appendix B of the Supplementary Information. Mean values ± standard error of the mean ($x \pm \sigma/\sqrt{N}$) of pressure (dbar), salinity, O_2 ($\mu mol \cdot kg^{-1}$), potential temperature □ (ºC) and Apparent Oxygen Utilization (AOU, $\mu mol \cdot kg^{-1}$) within each box are also shown as supporting information of the C_{ant} data.

3.3. Decadal trend and rate of change in C_{ant} storage

In order to study the temporal changes in the mean C_{ant} concentrations ($[C_{ant}]$) of φC_T^0, TrOCA and ΔC^* within each box for the period 1992-2011, an ensemble of 100 linear regressions between the five years and the 100 random-perturbed averages was obtained. Linear regressions for TTD were performed from 1992 to 2010. The mean and the standard deviation of the 100 linear regressions were considered as the Decadal Trend (DT) and the uncertainty (in µmol·kg^{-1} yr^{-1}) for [C_{ant}]) inside each box. (Table C1 in Appendix C). As each C_{ant} method yields a specific DT, hereafter they will be denoted as DT (method), e.g. DT(φC_T^0), DT(TrOCA), DT(ΔC*) and DT(TTD). Table C1 in the Supplementary Information shows the DT values in each box, per method.

Tanhua et al. (2006) found that C_{ant} is in transient steady state (TSS) in the North Atlantic from comparison of the observed changes in C_T and CFC fields with those predicted from an eddy-permitting ocean circulation model. This means that C_{ant} increases over time through the whole water column in a manner that is proportional to the time-dependent surface concentration. Hence, C_{ant} changes for a given time period can be determined from [C_{ant}] (Tanhua et al., 2007; Steinfeldt et al., 2009; Khatiwala et al., 2013; Pérez et al., 2013) considering the exponential fit $C^0_{(t)} = Ae^{\lambda t}$, that describes the history of atmospheric CO_2 and C^0_{ant} in the ocean surface mixed layer since the Industrial Revolution. Steinfeldt et al. (2009) reported an increase rate of 1.69% for the factor λ(yr^{-1}), for characteristic NADW properties. The uncertainty associated to λ was found to be 0.10%, based on the variability found between 1992 - 2012 in the estimated rates of C^0_{ant} increase in the surface mixed layer. The C_{ant} storage rate (µmol·kg^{-1}·yr^{-1}) under a transient steady state can be calculated within each box as the product between λ (yr^{-1}) and [C_{ant}] (µmol·kg^{-1}), being the term [C_{ant}] variable depending on the method used to estimate C_{ant}:

$$\frac{dC_{ant}}{dt} = \lambda \cdot [C_{ant}] \qquad (1)$$

To obtain robust $\frac{dC_{ant}}{dt}$ within each box, an ensemble of 100 $\frac{dC_{ant}}{dt}$ were obtained per each cruise via equation (1), from the 100 random-perturbed averages ([$C_{ant}^{\varphi C_T^0}$], [C_{ant}^{TrOCA}], [$C_{ant}^{\Delta C^*}$], [C_{ant}^{TTD}]) obtained as reported above and also considering the random perturbation of λ. Since all the cruises were grouped off to increase the amount of $\frac{dC_{ant}}{dt}$ estimations, the 100 random-perturbed averages relative to each cruise were previously time-normalized (Khatiwala et al., 2013) to the year 2000, via equation 2:

$$C_{(t2)} = C_{(t1)} e^{\lambda (t2 - t1)} \qquad (2)$$

where t1 corresponds to each A05 cruise occupation year and t2 is the reference year 2000. $C_{(t1)}$ corresponds to [C_{ant}] in each cruise, and $C_{(t2)}$ to the one normalized to year 2000. The temporal rescaling was performed to reduce the variability in the obtained storages due to the difference in [C_{ant}] between years, obtaining TSSR storages that were set in the middle of the studied period. The TSSR and its uncertainty were considered as the mean and standard deviation of the 500 $\frac{dC_{ant}}{dt}$ (100 per cruise). Hereafter, the C_{ant} storage rates (µmol·kg^{-1} yr^{-1}) computed following the Transient Stationary State approximation will be denoted as TSSR (method), e.g. TSSR(φC_T^0), TSSR(TrOCA), TSSR(ΔC^*) and TSSR(TTD). Table C1, in the Supplementary Information, shows the TSSR values in each box, per method. Taking into account that sometimes the C_{ant} estimates from different methods extend over a broad range of values, Khatiwala et al., (2013) suggesed that a combination of C_{ant} estimation methods, each with its own strengths and weaknesses, should be necessary to achieve a robust quantification of the ocean sink of C_{ant}. By applying their consideration to the C_{ant} storage, table C1 shows the mean DT and TSSR within each box, where the four methods used to compute C_{ant} are combined. Since DT uncertainties were more variable, the averaging was done by weighting the back-calculations with respect to the tracer method. The time-normalized [C_{ant}] (to year 2000) obtained averaging the four methods estimates is also shown.

4. Results

4.1. Modern C_{ant} distribution

Figure 2 shows the average distributions of $C_{ant}^{\varphi C_T^0}$ in 1992 and 2011, for the eastern and western basins separately. All profiles show a common overall shape in space and time, with higher $C_{ant}^{\varphi C_T^0}$ values near the surface that decrease towards the bottom. The vertical gradient is really strong in the upper ocean, from 150 to 1000 dbar, whilst concentrations remain low and almost constant deeper than this. Below 1000 dbar, only the DWBC contributes to the deep ocean ventilation, mostly through the LSW spreading pathway. Its role can be identified as the relative maximum in $C_{ant}^{\varphi C_T^0}$ between 1100 and 1800 dbar, in the western basin. Temporal differences in the profiles reveal a systematic full-depth enrichment in $C_{ant}^{\varphi C_T^0}$ in both basins that is substantially greater in the first 1000 dbar. These pressure ranges encompass the three uppermost density layers. Among them, uNACW and lNACW, which are formed at relatively close subtropical and temperate latitudes, show the largest accumulation detected in the water column, in a similar magnitude in each basin. Instead, in the deep ocean the $C_{ant}^{\varphi C_T^0}$ penetration occurs faster in the western than in the eastern basin due to the DWBC spreading. The $C_{ant}^{\varphi C_T^0}$ increase is larger between 1000 and 2000 dbar, while it is difficult to differenciate changes below that level to the bottom as the uncertainty estimates overlap (Fig.2).

4.2. Decadal Trends in C_{ant} storage by layers

4.2.1. uNACW ($\sigma_0 < 26.5$ kg m^{-3})

The four C_{ant} methods show the greatest [C_{ant}] of the whole water column in *uNACW*, as it is the most ventilated layer (Fig.3). The range in [C_{ant}] during the 1992 - 2011 period is wide and depends on the method used, suggesting a rise of about ~ 10 - 22 µmol·kg^{-1}. The four methods show consistent DT values between them in the eastern basin (R3 and R4, Fig. 4) but different DT in the C_{ant} accumulation of the western basin (R1 and R2). There, DT(TTD) indicates much lower decadal increases in [C_{ant}^{TTD}] than any DT obtained by using back-calculation methods. Thus, while [$C_{ant}^{\varphi C_T^0}$], [C_{ant}^{TrOCA}] and [$C_{ant}^{\Delta C^*}$] are estimated to have been increasing up to nearly ~ 1 µmol·kg^{-1} yr^{-1}, [C_{ant}^{TTD}] shows a decadal increase quite below this amount (DT and TSSR values are reported in table C1 of the Supplementary Information). The TTD method typically produces the highest estimates in the upper layers (Vázquez-Rodríguez et al., 2009a; Khatiwala et al., 2013). However, [C_{ant}^{TTD}] show a noticeably common change with time (Fig. 3) along the entire layer: a systematically changing offset with respect to the other three estimations from 1992 onwards, whereas the offset remains generally constant between cruises in the layers below. This can presumably be attributed to the decline in the atmospheric CFC concentrations since their peak during the past decade (Tanhua et al., 2008), which would lead to an even greater underestimation of [C_{ant}^{TTD}] in this layer (the most recently ventilated) moving closer to the end of the studied period.

4.2.2. lNACW (26.5< σ_0 < 27.1 kg m^{-3})

Regardless of the cruise, $[C_{ant}^{\varphi C_T^0}]$, $[C_{ant}^{TrOCA}]$, $[C_{ant}^{\Delta C^*}]$ and $[C_{ant}^{TTD}]$ are in general higher moving towards the east along the *lNACW*, coinciding with a higher ventilation due to the tilting of the isopycnal (Fig. 3). This layer shows a continuous and considerable increase in $[C_{ant}]$, of about ~ 6 to 11 µmol·kg^{-1}, when considering the four methods. The four methods agree in pointing to R4 as the region with the highest storage at these depth ranges (Fig. 4). Close to the western margin (R1), DT(TTD) suggests lower storage than back-calculations, which could also be explained as in the layer above, from the decline in the atmospheric CFC concentrations and the intense mixing with the layer above due to the winter outcrop (Bates, 2012).

4.2.3. AAIW (27.1< σ_0 < 27.5 kg m^{-3})

The four methods agree in showing a higher storage in R1 compared with the remaining regions (Figure 4). Moreover, DT(φC_T^0), DT(TrOCA) and DT(TTD) results show a similar longitudinal pattern: their high DT in R1 is reduced in the ocean interior (R2-R4) until quite similar DT values in R2 and R4 and a near absence of significant accumulation in R3. A noticeable exception concerns the stabilization of $[C_{ant}^{\varphi C_T^0}]$ and $[C_{ant}^{TrOCA}]$ in R3 (Fig. 3), which seems a real feature and not an artefact from the methodologies used, since $[C_{ant}^{TTD}]$ do not show either changes in time. However, the values of DT(TTD) are low in general compared to back-calculations (Fig. 4). DT(ΔC^*) results mostly coincide with this zonal pattern but suggest a considerable increase in $[C_{ant}^{\Delta C^*}]$ in R3 and R4. It is important to remark that determining C_{ant} in this layer is particularly difficult for a number of reasons. The *AAIW* layer encompasses characteristic biogeochemical singularities, it includes the O_2 minimum layer, for instance, and it is strongly influenced by the dynamic water mass front between *AAIW* and MW and the coastal upwelling (Brown *et al.*, 2010). Alltogether, the different behaviour in $[C_{ant}^{\Delta C^*}]$ could be related to the fact that this method appears to be more sensitive than the other methods to changes in □ and O_2 horizons shifts that occur in R3 and R4, in AAIW and uNADW (tables B3 and B4 in the Supplementary Information), which could have an effect on the computation of the disequilibrium term in these regions. Thus, a number of factors make inherently difficult to correctly compute [C_{ant}] or interpret its decadal trend at these depth ranges. Moreover, the fact that the temporal evolution of the C_{ant} averages along the *AAIW* layer practically parallels that of *uNADW* (Fig. 3) suggests that it might also be somewhat influenced by the LSW C_{ant} ventilation. Steinfeldt et al., (2007) also found a noticeable increase in the CFC-12 concentration with time close to the western boundary, at depth ranges right above the layer where the LSW spreads.

4.2.4. uNADW (σ_0> 27.5 and σ_2<37 kg m^{-3})

The DT results from the four methods highlight a significantly higher accumulation in R1 with respect to the remaining regions of the layer (Fig. 4), of up to ~ 8 to 11 µmol·kg^{-1}, due to the LSW penetration into the section. The DT values in R1 are consistent with, or even higher than in the layer above, with the four values amounting to ~ 0.5 µmol·kg^{-1} yr^{-1}. This value confirms the important C_{ant} advection in depth associated to the LSW, as it matches the yearly C_{ant} accumulation along *lNACW* and half of that along *uNACW*. As reported above, the DT(ΔC*) results are somewhat high compared with the other three methods in the eastern basin (Fig. 4), giving to significant storages along the entire layer. Instead, a significantly lower accumulation of [$C_{ant}^{\varphi C_T^0}$], [C_{ant}^{TrOCA}] and [C_{ant}^{TTD}] appears to take place in R4 (at least half of that in [$C_{ant}^{\Delta C^*}$]), whereas no increase in any of them occurred in R3.

4.2.5. lNADW (σ_2> 37 and σ_4<45.9 kg m^{-3})

As shown in Figure 3, [$C_{ant}^{\Delta C^*}$], [$C_{ant}^{\varphi C_T^0}$], [C_{ant}^{TrOCA}] and [C_{ant}^{TTD}] are different in magnitude in some regions but, nonetheless, their temporal trends do suggest relatively consistent results (Fig. 4). DT values from the four methods agree in showing a significant, albeit low, decadal increase in [C_{ant}] in R1, that amounts to about half of the annual increase in the layer above. ΔC* and TTD methods agree in suggesting significant [C_{ant}^{TTD}] and [$C_{ant}^{\Delta C^*}$] accumulation in the entire western basin, while φC_T^0 and TrOCA do not indicate any build-up in R2 (Fig. 4). In the eastern basin, none of the methods indicates accumulation of C_{ant} during the last two decades, despite the fact that significant mean concentrations are exhibited (Fig. 3).

4.2.6. AABW (σ_4>45.9 kg m^{-3})

In this layer, [C_{ant}] changes in time appear to be negligible in general (Fig. 3). Although the C_{ant} content can be considered to be significant by the four methods (mostly from 2004 on), the error bars are too high to confirm a significant rise in their concentrations. In R1, DT(φC_T^0) and DT(TrOCA) results suggest a low accumulation from back-calculation methods, while [C_{ant}^{TTD}] remain almost constant in time (Fig. 4). Regarding R2, DT results neither reveal any changes during the last two decades. That could be related to the quantification limits of the methods, as in the layer above, making difficult to evidence, during a bi-decadal period, the slow increase of the really diluted C_{ant} signal by the time it arrives at these latitudes. Alternatively, ir could be related, to the more pristine characteristics of the *AABW*.

4.2.7. Florida Strait

As shown in Figure 3, [C_{ant}] increases are observable in the three layers that move though the FS. Although higher variability is found in the [C_{ant}] estimates within the FS, DT results in this region show, in general, a higher accumulation than in R1 in central waters (*uNACW* and l*NACW*). However, the values in the *AAIW* layer suggest a lower accumulation than in R1 that is really noticeable when using the TTD method. According to Schmitz and Richardson (1991), the vertical pattern with regard to the main section could be explained by the respective origins of the three layers entering the FS. The *uNACW* and *lNACW* find its origin at closer latitudes, in relation with the recirculation of the North Equatorial Current. In contrast, the *AAIW* layer in the FS proceeds directly from the South Eastern Atlantic. While the two uppermost layers show similar □/*S* and oxygen values with the next region, the *AAIW* shows respectively lower □/*S* and higher AOU values than those in the main section (tables in Appendix B of the Supplementary Information). Thus, DT(TTD) suggests lower decadal increases than back-calculation methods (Fig. 4), as there is no increase in $[C_{ant}^{TTD}]$ during the last two decades. DT results by using back-calculation methods show consistent values between TrOCA and ΔC* in the FS. DT(φC_T^0) are slightly lower in the two first layers while it is consistent with them in the *AAIW* layer.

4.3. TSSR C_{ant} storage rates by layers

Purple dashed lines in Figure 3 correspond to the mean TSSR reported in Table C1 of Appendix C, taking into account its confidence interval. Long-term storage (TSSR) results indicate the expected storage according to the [C_{ant}] levels found in each box taking into account the exponential fit of the C_{ant} accumulation in the surface ocean on long time scales. Thus, TSSR values follow the [C_{ant}] distribution (i.e. boxes containing the greater concentrations exhibit the highest storages, and the accumulation rates decrease in depth or along the different layers according to the progressively lower concentrations). TSSR results are in general more consistent between the four methods than they are from the DT approach, which indicates that $[C_{ant}^{\varphi C_T^0}]$, $[C_{ant}^{TrOCA}]$, $\left[C_{ant}^{\Delta C^*}\right]$ and $[C_{ant}^{TTD}]$ estimations are, actually, very close between them. However, TSSR results do not always match those obtained from the DT approach (Fig. 4). They also show much lower uncertainties than the DT approach, mainly in the deep ocean, due to the time-normalization of the data. This is the main benefit of using the TSSR approach. By referring the mean [C_{ant}] of the five cruises to the year 2000 (values in table C1 in the Supplementary Information), possible biases in any dataset are smoothed from the averaging with the other ones. Thus, the uncertainties of the obtained storages are reduced, making them more robust. In contrast, the DT approach is more sensitive to the data quality from each cruise, taking into account that few averages (n=5) are used to perform the linear regressions. However, the DT approach allows the detection of a more realistic C_{ant} storage in relation to the specific bi-decadal period of study, since changes are computed only considering data from this time period. Conversely, TSSR results need to be interpreted in terms of a previous accumulative history of the estimated [C_{ant}] due to the fact that the storage is computed based on the assumption of the observed C_{ant} increase in the surface since the preindustrial era that follows an exponential fit. Thus, possible real variations in [C_{ant}] increase which deviate from a steady-state accumulation could become masked in the TSSR results due to its integration into the past accumulative history of C_{ant}. Comparisons between the two approaches are helpful to interpret the observed temporal changes in [C_{ant}], especially if these changes can be compared between estimations obtained following both CO_2 (back-calculation) and tracer based methods. When the outputs of both approaches (DT and TSSR) coincide, this could be interpreted as situations in which the more punctual or short-term (here bi-decadal) C_{ant} storage (i.e. the DT) is confirmed with the integrated or long-term (centennial) C_{ant} storage (i.e. the TSSR).

4.3.1. The upper ocean: uNACW, lNACW and AAIW

Central Waters (*uNACW* and *lNACW*) show progressively higher TSSR values from R1 to R4 (Fig. 4), suggesting a higher expected storage in the eastern than in the western basin. This pattern is in accordance with the [C_{ant}] distributions along the layers. In the *uNACW*, TSSR and DT results from any method are fairly coincident in R4. However, the storages obtained from both approaches start to differ while moving towards the west (R1): in one hand, TSSR values from the three back-calculation methods slightly decrease moving from R3 to R1 (as [C_{ant}] do) but their analogous DT remain more or less equal (φC_T^0) or even increase (TrOCA or ΔC^*) in that direction (Fig. 4). On the other hand, the observed DT(TTD) values suggest a lower [C_{ant}^{TTD}] accumulation towards the west while TSSR(TTD) results indicate that a quite similar accumulation should be expected along the layer. The noticeable difference between DT and TSSR approaches is significant for the four methods in the western basin. While DT(TTD) suggest that [C_{ant}^{TTD}] has been accumulating slower than expected from the inventory, at least during the last two decades, DT(φC_T^0), DT(TrOCA) and DT(ΔC^*) results suggest the contrary for [$C_{ant}^{\varphi C_T^0}$], [C_{ant}^{TrOCA}], [$C_{ant}^{\Delta C^*}$], which have increased their values in the basin more substantially than would have been expected from a steadier behavior. In contrast to this, the eastern basin shows decadal trends closer to a more stationary build-up. In water masses below, the most noticeable feature along the *lNACW* is the strongest longitudinal gradient in the storage rates between the eastern (higher) and the western (lower) basins suggested from TSSR results in comparison with the DT results that are more consistent along the entire layer. This is due to the strong gradient in [C_{ant}] associated to the shallowing of the isopycnals towards the east. However, only DT(TTD) shows the same pattern since DT from back-calculation methods, in general, are more similar along the layer. In the *AAIW*, TSSR values from the four methods are really close between them and indicate very similar storages along the entire layer (Fig. 4). A noticeable common feature is that no method suggests an expected greater accumulation in the DWBC region (R1) compared with the remaining layer, as their relative DT results indicate. The expected TSSR storages in the ocean interior (R2 to R4) are mostly similar between the TTD and the back-calculated TSSR results, which is not paralleled always in the DT(TTD) values, that are low in general. The TSSR storages found from R2 to R4 are consistent to the observed DT values for φC_T^0 and TrOCA. The only mismatch occurs in R3 where a TSSR storage similar to the surrounding regions is expected, as the C_{ant} concentrations are significant, but neither $[C_{ant}^{\phi C_T^0}]$, nor $[C_{ant}^{TrOCA}]$ nor $[C_{ant}^{TTD}]$ actually appear to have been increasing during the two decades.

4.3.2. The deep ocean: uNADW, lNADW and AABW

In the deep layers (*uNADW* and *lNADW*) both approaches coincide in pointing out R1 as the leading region in the C_{ant} build-up with respect to the ocean interior. However, TSSRs results exhibit a softer zonal gradient in the storage rates along the section than their respective DT values (Fig.4), mostly in the *uNADW*. This result highlights the significant role of the DWBC on the observed [C_{ant}] entrance in the deeper western basin and the noticeable contribution of the LSW to this penetration during the period of study. The boxes of the ocean interior where [C_{ant}] are close to the detection limits show low but significant TSSR storages (Fig. 4). Opposite to this, their related DT values are not always significant. This might be related to the inherent difficulty to accurately estimate the C_{ant} levels in deep waters and also to its (slow) temporal increase, as they are assumed to contain very low concentrations that are quite close to the detection capacity of the methods. It is thus difficult to ascertain if the absence of rising [C_{ant}] observed in the deep ocean interior (mainly in the *lNADW)* is real or, as reported above, just a consequence of the time series not being long enough in duration. This restriction is also relevant for the *AABW*, where TSSR and DT approaches do describe consistent storages in R1, indicating the likely [C_{ant}] presence and its increase at very low rates (significant from φC_T^0 and TrOCA) in old waters close to the bottom. The C_{ant} build-up could be considered to be occurring in R2 as well, according to the coincidence of the TSSR results with those in R1.

5. Discussion

The mean TSSR storage rate for the whole *uNACW* layer, considering the results obtained with the four methods, gives an expected accumulation of 0.84 ± 0.07 µmol·kg^{-1} ·yr^{-1}. The equivalent mean DT suggests a slightly higher observed value of 0.93 ± 0.09 µmol·kg^{-1}·yr^{-1} (Fig. 4) that is mostly influenced by the significant dissimilarity between the two approaches in the western basin, opposite to the eastern one, that shows DT values closer to a steadier accumulation. DT results from the back-calculation methods make the difference, indicating a significant higher storage than expected in the uppermost layer (1.07±0.08 µmol·kg^{-1} ·yr^{-1} on average) mainly due to the high storage found in FS, R1 and R2 (1.10±0.07 µmol·kg^{-1} ·yr^{-1}) with respect to that in R3 and R4 (0.98±0.12 µmol·kg^{-1} ·yr^{-1}). Our findings are in accordance with those reported in the time series stations in the Subtropical North Atlantic. Observations at BATS (Bermuda Atlantic Time-series Study), situated in the Western Subtropical North Atlantic, suggest a three-decade trend (1983-2011) of 1.08 ± 0.06 µmol·kg^{-1} ·yr^{-1} for surface salinity-normalized C_T (nC_T) (Bates et al., 2012). Conversely, at ESTOC (European Times Series Canary Islands), situated opposite to BATS in the Eastern basin, a surface nC_T storage rate of 0.99 ± 0.20 µmol·kg^{-1}·yr^{-1} was reported (1995-2004) (Santana-Casiano et al., 2007). Although both values indicate an equivalent nC_T storage taking into account error bars, a slightly faster nC_T accumulation could be suggested for the western basin. In addition, the particular C_{ant} storage rate for Subtropical Mode Water (the main component of the *uNACW* layer in the western basin) was estimated at 1.06 µmol·kg^{-1}·yr^{-1} between 1988 and 2011 (Bates, 2012). In ESTOC, a C_{ant} storage rate of 0.85 ± 0.6 µmol·kg^{-1}·yr^{-1} was reported for the first 200m, matching the observed increase in nC_T (0.85 ± 0.16 µmol·kg^{-1}·yr^{-1}) for the seasonal thermocline (about 120 meters) (González-Dávila et al., 2010). Moreover, net CO_2 air-sea fluxes of -0.81 ± 0.25 to – 1.3 ± 0.3 mol·m^{2}·yr^{-1} (1983 – 2005) and -0.051 ± 0.036 to – 0.054 ± 0.03 mol·m^{2}·yr^{-1} (1995 – 2004), reported respectively for BATS (Bates, 2007) and ESTOC (Santana-Casiano et al., 2007), would also indicate that the eastern side of the NASTG has been acting as a much weaker sink of atmospheric CO_2 compared to the BATS site. These findings are consistent with previous results where BATS was found to be in a region of strong spatial gradients in air-sea CO_2 flux (Nelson et al., 2001). These results support our finding that during the last two decades C_{ant} might have been absorbed more intensely in the western side of the NASTG. Circulation patterns would support these findings as STMW water that forms near the Sargasso Sea recirculates near the formation site and also travels to the eastern NASTG through the Azores Current (Schmitz and Richardson, 1991; Follows et al., 1996). Larger amounts of CO_2 entering into the ocean near Bermuda, according to the larger CO_2 fluxes described (Bates, 2007), would be thus advected to the opposite part of the section below the surface. The arrival of C_{ant} enriched waters into the east could have an effect in both the lower uptake observed in the eastern side (Santana-Casiano *et al.*, 2007) and the higher [C_{ant}] described estimations (tables in appendix A). The winter outcrop in the west (Bates, 2012) could also favour lower [C_{ant}] of *lNACW* due to the mixing with the less saturated underlying waters. The mixing of *lNACW* with *uNACW* could be also responsible of the observed opposite TSSR and DT zonal gradients, thus supporting a higher C_{ant} uptake by central waters at the western side of the section.

Opposite to central waters that show a general sustained long-term increase in [C_{ant}] values over their whole extent during the last two decades, the layers below (*AAIW*, *NADW*, *AABW*) show a generalized contrasting behaviour between the DT results in R1 and those in the ocean interior (R2-R4). The DWBC influence extends to R2 in most layers, resulting in contrasting DT between the western and eastern basins as a whole. In *AAIW*, the greater rise in concentrations appears to occur in the western basin. (Brown *et al.*, 2010) pointed out that the variability in [C_{ant}] at these intermediate depths most likely results from changing mixing characteristics of waters of southern and Mediterranean origin, mainly due to a lateral movement of the water mass front that occurs between the *AAIW* and the *MW*. Regardless of the modulation of the C_{ant} budget from the *MW* spreading (Álvarez et al., 2005), the eastern basin shows almost no (R3) or slight (R4) [C_{ant}] changes in time, which indicates that the observed DT storage rate for the whole *AAIW* (0.22 ± 0.08 $\mu mol \cdot kg^{-1} \cdot yr^{-1}$) might have been mainly driven by R1. Although the higher DT in R1 represents a relative minimum compared to those in *uNACW* and *uNADW* in the same region, it might have been mainly influenced by the C_{ant} signal of the LSW spreading underneath (Steinfeldt *et al.*, 2007). The prevailing role of R1 in the full section storage variability on decadal scale becomes much more evident in deep waters below 1000 dbar (Macdonald et al., 2003; Brown et al., 2010). In R1 the storage rates in *uNADW and lNADW* are significantly higher than those in R2 to R4 (Fig. 4). This is the region influenced by the DWBC (Fig. 2), which is C_{ant} loaded (Steinfeldt et al., 2009; Pérez et al., 2010a) with respect to the less-ventilated layers that recirculate in the ocean interior, which show small (*uNADW*) or not significant (*lNADW*) DT values.

Regarding *AABW*, weighted DT results in R1 also show a non significant trend of about 0.11 ± 0.14 $\mu mol \cdot kg^{-1} \cdot yr^{-1}$ (Fig. 4), while those in R2 suggest no increase in [C_{ant}]. However, the corresponding TSSR values (0.12 ± 0.05 $\mu mol \cdot kg^{-1} \cdot yr^{-1}$ in R1 and 0.11 ± 0.04 $\mu mol \cdot kg^{-1} \cdot yr^{-1}$ in R2) suggest similar storages for the whole layer that are in turn equivalent to the observed DT results in R1. Ríos et al. (2012) reported a significant C_{ant} storage rate of 0.15 ± 0.04 $\mu mol \cdot kg^{-1} \cdot yr^{-1}$ (1971 to 2003) in *AABW* in the Western South Atlantic (55°S-10N). For this same basin, Wanninkhof et al. (2013) were able to detect small C_T changes, from pCO_2 measurements, in deep waters from 44°S to the Equator, obtaining a storage rate of 0.47 $mmol \cdot m^{2} \cdot yr^{-1}$ for depths under 2000 m. Considering an average thickness for the water column of about ~3000 m (from ~2000 m to the ocean bottom) it can be deducted that they found storage rates equivalent to ~0.15 $\mu mol \cdot kg^{-1} \cdot yr^{-1}$, that are applicable to deep and bottom water masses at these latitudes in the North Atlantic, in agreement with Ríos et al.(2012). Both results are consistent with the mean TSSR values obtained in the *AABW* (table C1 in Appendix C) which indicate the expected storage according to the estimated [C_{ant}] in this layer. Only the weighted DT in R1 appears to confirm this. In addition, a mean TSSR of 0.12 ± 0.05 $\mu mol \cdot kg^{-1} \cdot yr^{-1}$ is also obtained for the whole *lNADW* layer, which is also consistent to Ríos et al. (2012) and Wanninkhof et al. (2013). Only DT(TTD) and DT(ΔC^*) suggest a similarly observed result for the *lNADW* layer in R2 (table C1 in Appendix C). Brown et al. (2010) described a significant nonzero C_{ant} signal at 24.5°N for depth ranges between 4000 - 6000 dbar in the deep eastern basin (Fig 7 in Brown et al.(2010)), that was confirmed from CCl_4 measurements). The authors suggested that those [C_{ant}] levels might be related to the arrival of ventilated waters from the North along the eastern flank of the Mid-Atlantic Ridge, which (Paillet and Mercier, 1997) described as Iceland-Scotland Overflow Water. Roughly, it would correspond to and approximate storage of about ~ 0.2 - 0.3 $\mu mol \cdot kg^{-1} \cdot yr^{-1}$, which is consistent with our results, given the fact that our storage is referred to a layer with almost double thickness (between 2500- 5500) dbar.

6. Conclusions

The 2010 and 2011 most recent occupations of the A05 section, across 24.5°N in the Subtropical North Atlantic, were put into historical context with respect to their CO_2 system measurements through comparison with data of three previous cruises. The five A05 repeated sections permitted the estimation of the C_{ant} storage on decadal timescales, taking into account changes in circulation during this period. To better constrain the accumulation of C_{ant}, this was estimated by using four different methods that include back-calculation (ΔC^*, TrOCA and φC_T^0) and tracer (TTD) principles. Regardless of the method used to estimate [C_{ant}], the overall distribution showed higher C_{ant} concentrations near the surface that decreased towards the bottom. From the study of the C_{ant} accumulation along the different water masses found in the section, we found that the greatest decadal storage rates were observed in the central water masses: the *uNACW* showed a mean storage rate close to ~1 $\mu mol \cdot kg^{-1} \cdot yr^{-1}$ and the *lNACW* displayed half of that (~0.5 $\mu mol \cdot kg^{-1} \cdot yr^{-1}$) on average. Our results along the *uNACW* are also in accordance with the reported storage rates of C_{ant} and nC_T for BATS (Bates, 2012) and ESTOC (González-Dávila *et al.*, 2010) time series stations and suggest that during the last two decades C_{ant} might have been absorbed more intensely in the western side of the NASTG. Below the central layers, neither intermediate nor deep water masses showed average storage rates greater than ~0.25 $\mu mol \cdot kg^{-1} \cdot yr^{-1}$. However, the four methods gave evidence of the strong zonal gradient in the C_{ant} storage rates below 1000 dbar, in which the western basin presented a noticeable C_{ant} accumulation close to the continental margin due to the conveyer role of the DWBC, in comparison with the low storage rates of the ocean interior. In particular, the storage rate of the *uNADW* within the DWBC region amounted to ~0.5 $\mu mol \cdot kg^{-1} \cdot yr^{-1}$ due to the great ventilation by the LSW.

In general, the four methods gave consistent storage rates indicating a good agreement between tracer and CO_2-based results. However, some differences in the obtained storage rates were observed: the TTD method may lead give to underestimated storages in the uppermost layer (*uNACW*), likely because of the decrease in the atmospheric CFC concentrations after 1992. During our studied period, CFCs would not be a proper proxy to track the atmospheric C_{ant} increase in the younger water masses, while would it not compromise the older ones. The ΔC^* method suggested decadal storage values slightly higher than the other three methods in the eastern basin in intermediate and deep layers, which likely results from the estimation of its disequilibria. The C_{ant} accumulation by using TrOCA method usually fells between ΔC^* and φC_T^0 results, with the last method indicating storage rates closer to the TTD method. There was generally better agreement between the storage rates of the four methods in the layers where the estimation of C_{ant} is more robust. Differences between the storage rates found between methods were more evident where the C_{ant} detection limits became more important. In deep homogeneous waters with very low C_{ant}, absolute uncertainties were of the same order of magnitude as the C_{ant} concentrations, making significant trends difficult to separate from the background noise on a timescale of two decades. This is the case of most *lNADW* and *AABW*, where there was no obvious accumulation of C_{ant} considering the uncertainties, despite the fact that the estimated C_{ant} content could be considered to be significant. Here, we found significant bi-decadal trends in the C_{ant} storage rates of the deepest Subtropical North Atlantic waters by using all five A05 datasets and the assumption of a transient steady state of the C_{ant} distributions, in order to reduce the uncertainties related to deep waters measurements. Our results are consistent with Ríos et al. (2012) who used the same methodology than our study (C_T and A_T measurements) but a larger timescale (three decades) to compute the C_{ant} storage in the Western South Atlantic basin. Our findings also match those obtained by Wanninkhof et al. (2013), who studied the C_{ant} change along the entire Atlantic Ocean during a period of time similar to ours, almost two decades, though with more precise pCO_2 measurements.

The A05 repeat hydrography thus permits the robust estimation of the storage of C_{ant} on decadal timescales and allows a better constraint of the interactions between the ocean circulation and the carbon cycle, in particular regarding the mechanisms governing the accumulation of C_{ant} along the Subtropical North Atlantic.

Acknowledgements

We would like to thank captains, officers and crews of RRS Discovery and R/V Sarmiento de Gamboa and the scientific and technical teamsfor their support and indispensable help during the cruises in 2010 and 2011. We acknowledge funding from the Spanish Ministry of Economy and Competitiveness through grants CSD2008-00077 (Circumnavigation Expedition MALASPINA 2010 Project), CTM2009-08849 (ACDC Project) and CTM2012-

32017 (MANIFEST Project) and from the 7th Framework Programme FP7 CARBOCHANGE, C-ENVIR/0869. We also acknowledge funding from EU CARBOCHANGE project (264879). E.F. Guallart was funded by CSIC through a JAE-Pre grant.

References

Álvarez, M., Pérez, F.F., Shoosmith, D.R., Bryden, H.L., 2005. Unaccounted role of Mediterranean Water in the drawdown of anthropogenic carbon. Journal of Geophysical Research: Oceans (1978–2012), 110.

Álvarez, M., Ríos, A.F., Pérez, F.F., Bryden, H.L., Rosón, G., 2003. Transports and budgets of total inorganic carbon in the subpolar and temperate North Atlantic. Global Biogeochemical Cycles, 17, 1002.

Anderson, L.A., Sarmiento, J.L., 1994. Redfield ratios of remineralization determined by nutrient data analysis. Global Biogeochemical Cycles, 8, 65-80.

Bates, N.R., 2007. Interannual variability of the oceanic CO2 sink in the subtropical gyre of the North Atlantic Ocean over the last 2 decades. Journal of Geophysical Research: Oceans, 112, C09013.

Bates, N.R., 2012. Multi-decadal uptake of carbon dioxide into subtropical mode water of the North Atlantic Ocean. Biogeosciences, 9, 2649-2659.

Bates, N.R., Best, M.H.P., Neely, K., Garley, R., Dickson, A.G., Johnson, R.J., 2012. Detecting anthropogenic carbon dioxide uptake and ocean acidification in the North Atlantic Ocean. Biogeosciences 9, 2509-2522.

Brewer, P.G., 1978. Direct observation of the oceanic CO2 increase. Geophysical Research Letters, 5, 997-1000.

Broecker, W.S., Peng, T.H., 1974. Gas exchange rates between air and sea. Tellus, 26, 21-35.

Brown, P.J., Bakker, D.C.E., Schuster, U., Watson, A.J., 2010. Anthropogenic carbon accumulation in the subtropical North Atlantic. Journal of Geophysical Research-Oceans, 115, 4016.

Castaño-Carrera, M., Pardo, P.C., Álvarez, M., Lavín, A., Rodríguez, C., Carballo, R., Ríos, A.F., Pérez, F.F., 2012. Anthropogenic carbon and water masses in the bay of Biscay. Scientia Marina, 38, 191-207.

Chen, G.T., Millero, F.J., 1979. Gradual increase of oceanic CO2. Nature, 277, 205-206.

Clayton, T.D., Byrne, R.H., 1993. Spectrophotometric seawater pH measurements: total hydrogen ion concentration scale calibration of m-cresol purple and at-sea results. Deep Sea Research Part I: Oceanographic Research Papers, 40, 2115-2129.

Cunningham, S.A., 2005. Cruise Report No. 54. RRS Discovery Cruise D279, 04 Apr - 10 May 2004. A Transatlantic hydrographic section at 24.5ºN. . Southampton Oceanography Centre.

Dickson, A.G., Sabine, C.L., Christian, J.R., 2007. Guide to best practices for ocean CO_2 measurements.

Fajar, N.M., Pardo, P.C., Carracedo, L., Vázquez-Rodríguez, M., Ríos, A.F., Pérez, F.F., 2012. Trends of anthropogenic CO2 along 20°W in the Iberian Basin. Scientia Marina, 38, 287-306.

Flecha, S., Pérez, F.F., Navarro, G., Ruiz, J., Olivé, I., Rodríguez-Gálvez, S., Costas, E., Huertas, I.E., 2012. Anthropogenic carbon inventory in the Gulf of Cádiz. Journal of Marine Systems, 92, 67-75.

Follows, M.J., Williams, R.G., Marshall, J.C., 1996. The solubility pump of carbon in the subtropical gyre of the North Atlantic. Journal of Marine Research, 54, 605-630.

González-Dávila, M., Santana-Casiano, J.M., Rueda, M.J., Llinás, O., 2010. The water column distribution of carbonate system variables at the ESTOC site from 1995 to 2004. Biogeosciences 7, 3067-3081.

Goyet, C., Coatanoan, C., Eischeid, G., Amaoka, T., Okuda, K., Healy, R., Tsunogai, S., 1999. Spatial variation of total CO_2 and total alkalinity in the northern Indian Ocean: A novel approach for the quantification of anthropogenic CO_2 in seawater. Journal of Marine Research, 57, 135-163.

Gruber, N., Sarmiento, J.L., Stocker, T.F., 1996. An improved method for detecting anthropogenic CO2 in the oceans. Global Biogeochemical Cycles, 10, 809-837.

Guallart, E.F., Pérez, F.F., Rosón, G., Ríos, A.F., 2013. High spatial resolution alkalinity and pH measurements by IIM-CSIC group along 24.5°N during the R/V Hespérides WOCE Section A05 cruise. (July 14 - August 15, 1992). Oak Ridge, Tennessee: Carbon Dioxide Information Analysis Center, Oak Ridge National Laboratory, US Department of Energy.

Haine, T.W.N., Hall, T.M., 2002. A Generalized Transport Theory: Water-Mass Composition and Age. Journal of Physical Oceanography, 32, 1932.

Heinze, C., 2004. Simulating oceanic CaCO3 export production in the greenhouse. Geophysical Research Letters, 31, L16308.

Johns, W.E., Baringer, M.O., Beal, L.M., Cunningham, S.A., Kanzow, T., Bryden, H.L., Hirschi, J.J.M., Marotzke, J., Meinen, C.S., Shaw, B., Curry, R., 2011. Continuous, Array-Based Estimates of Atlantic Ocean Heat Transport at 26.5°N. Journal of Climate, 24, 2429-2449.

Johnson, K.M., Dickson, A.G., Eischeid, G., Goyet, C., Guenther, P., Key, R.M., Millero, F.J., Purkerson, D., Sabine, C.L., Schottle, R.G., Wallace, D.W.R., Wilke, R.J., Winn, C.D., 1998. Coulometric total carbon dioxide analysis for marine studies: Assessment of the quality of total inorganic carbon measurements made during the US Indian Ocean CO2 survey 1994-1996. Marine Chemistry, 63, 21-37.

Khatiwala, S., Tanhua, T., Mikaloff Fletcher, S., Gerber, M., Doney, S.C., Graven, H.D., Gruber, N., McKinley, G.A., Murata, A., Ríos, A.F., Sabine, C.L., Sarmiento, J.L., 2013. Global ocean storage of anthropogenic carbon. Biogeosciences, 10, 2169-2191.

Körtzinger, A., Mintrop, L., Duinker, J.C., 1998. On the penetration of anthropogenic CO2 into the North Atlantic Ocean. Journal of Geophysical Research: Oceans, 103, 18681-18689.

Law, C.S., Watson, A.J., Liddicoat, M.I., 1994. Automated vacuum analysis of sulphur hexafluoride in seawater: derivation of the atmospheric trend (1970–1993) and potential as a transient tracer. Marine Chemistry, 48, 57-69.

Lo Monaco, C., Goyet, C., Metzl, N., Poisson, A., Touratier, F., 2005. Distribution and inventory of anthropogenic CO2 in the Southern Ocean: Comparison of three data-based methods. Journal of Geophysical Research C: Oceans, 110, 1-12.

Macdonald, A.M., Baringer, M.O., Wanninkhof, R., Lee, K., Wallace, D.W.R., 2003. A 1998–1992 comparison of inorganic carbon and its transport across 24.5°N in the Atlantic. Deep Sea Research Part II: Topical Studies in Oceanography, 50, 3041-3064.

Matsumoto, K., Gruber, N., 2005. How accurate is the estimation of anthropogenic carbon in the ocean? An evaluation of the ΔC* method. Global Biogeochemical Cycles, 19, GB3014.

McCartney, M.S., Talley, L.D., 1982. The Subpolar Mode Water of the North Atlantic Ocean. Journal of Physical Oceanography, 12, 1169-1188.

Mehrbach, C., Culberson, C.H., Hawley, J.E., Pytkowicz, R.M., 1973. Measurement of the Apparent Dissociation Constants of Carbonic Acid in Seawater at Atmospheric Pressure. Limnology and Oceanography, 18, 897-907.

Millero, F.J., Lee, K., Roche, M., 1998. Distribution of alkalinity in the surface waters of the major oceans. Marine Chemistry, 60, 111-130.

Mintrop, L., Pérez, F.F., Gonzalez-Dávila, M., Santana-Casiano, J.M., Körtzinger, A., 2000. Alkalinity determination by potentiometry: intercalibration using three different methods. Ciencias Marinas, 26(1), 23-27.

Nelson, N.B., Bates, N.R., Siegel, D.A., Michaels, A.F., 2001. Spatial variability of the CO2 sink in the Sargasso Sea. Deep Sea Research Part II: Topical Studies in Oceanography, 48, 1801-1821.

Paillet, J., Mercier, H., 1997. An inverse model of the eastern North Atlantic general circulation and thermocline ventilation. Deep Sea Research Part I: Oceanographic Research Papers, 44, 1293-1328.

Peltola, E., Lee, K., Wanninkhof, R., Feely, R., Roberts, M., Greeley, D., Baringer, M., Johnson, G., Bullister, J., Mordy, C., Zhang, J.-Z., P. Quay, F., Millero, F., Hansell, D., Minnett, P., 2001. Chemical and Hydrographic measurements on a climate and global change cruise along 24ºN in the Atlantic Ocean Woce Section A5R(repeat) during JAnuary-February 1998. Miami, Florida: Atlantic Oceanographic and Meteorological Laboratory. .

Pérez, F.F., Vázquez-Rodríguez, M., Mercier, H., Velo, A., Lherminier, P., Ríos, A.F., 2010a. Trends of anthropogenic CO2 storage in North Atlantic water masses. Biogeosciences, 7, 1789-1807.

Pérez, F.F., Aristegui, J., Vázquez-Rodríguez, M., Ríos, A.F., 2010b. Anthropogenic CO2 in the Azores region. Scientia Marina, 74, 11-19.

Pérez, F.F., Mercier, H., Vázquez-Rodríguez, M., Lherminier, P., Velo, A., Pardo, P.C., Rosón, G., Ríos, A.F., 2013. Atlantic Ocean CO2 uptake reduced by weakening of the meridional overturning circulation. Nature Geoscience, 6, 146-152.

Pierrot, D., Lewis, E., Wallace, D., 2006. MS Excel Program Developed for CO_2 System Calculations, ORNL/CDIAC-105a. Carbon Dioxide Information Analysis Center, Oak Ridge National Laboratory, US Department of Energy, Oak Ridge, Tennessee.

Ríos, A.F., Velo, A., Pardo, P.C., Hoppema, M., Pérez, F.F., 2012. An update of anthropogenic CO 2 storage rates in the western South Atlantic basin and the role of Antarctic Bottom Water. Journal of Marine Systems, 94, 197-203.

Rosón, G., Ríos, A.F., Pérez, F.F., Lavín, A., Bryden, H.L., 2003. Carbon distribution, fluxes, and budgets in the subtropical North Atlantic Ocean (24.5°N). Journal of Geophysical Research: Oceans, 108, n/a-n/a.

Sabine, C.L., Feely, R.A., Gruber, N., Key, R.M., Lee, K., Bullister, J.L., Wanninkhof, R., Wong, C.S., Wallace, D.W.R., Tilbrook, B., Millero, F.J., Peng, T.-H., Kozyr, A., Ono, T., Rios, A.F., 2004. The oceanic sink for anthropogenic CO_2. Science, 305, 367-371.

Sabine, C.L., Tanhua, T., 2010. Estimation of Anthropogenic CO2 Inventories in the Ocean. Annual Review of Marine Science, 2, 175-198.

Santana-Casiano, J.M., González-Dávila, M., Rueda, M.-J., Llinás, O., González-Dávila, E.-F., 2007. The interannual variability of oceanic CO2 parameters in the northeast Atlantic subtropical gyre at the ESTOC site. Global Biogeochemical Cycles, 21, GB1015.

Schmitz Jr.W.J., Richardson, P.L., 1991. On the sources of the Florida Current. Deep Sea Research Part A. Oceanographic Research Papers, 38, Supplement 1, S379-S409.

Schuster, U., Watson, A.J., Bakker, D.C.E., de Boer, A.M., Jones, E.M., Lee, G.A., Legge, O., Louwerse, A., Riley, J., Scally, S., 2013. Measurements of total alkalinity and inorganic dissolved carbon in the Atlantic Ocean and adjacent Southern Ocean between 2008 and 2010. Earth Syst. Sci. Data Discuss., 6, 621-639.

Smethie, W.M., Schlosser, P., Bönisch, G., Hopkins, T.S., 2000. Renewal and circulation of intermediate waters in the Canadian Basin observed on the SCICEX 96 cruise. Journal of Geophysical Research: Oceans, 105, 1105-1121.

Steinfeldt, R., Rhein, M., Bullister, J.L., Tanhua, T., 2009. Inventory changes in anthropogenic carbon from 1997–2003 in the Atlantic Ocean between 20°S and 65°N. Global Biogeochemical Cycles, 23, GB3010.

Steinfeldt, R., Rhein, M., Walter, M., 2007. NADW transformation at the western boundary between and. Deep Sea Research Part I: Oceanographic Research Papers, 54, 835-855.

Stendardo, I., Gruber, N., Körtzinger, A., 2009. CARINA oxygen data in the Atlantic Ocean. Earth system science data, 1, 87-100.

Talley, L.D., Pickard, G.L., Emery, W.J., Swift, J.H., 2011. Chapter 9 - Atlantic Ocean. *Descriptive Physical Oceanography (Sixth Edition)* (pp. 245-301). Boston: Academic Press.

823 Tanhua, T., Biastoch, A., Körtzinger, A., Lüger, H., Böning, C., Wallace, D.W.R., 2006. Changes of anthropogenic CO2 and CFCs in the North Atlantic between 1981 and 2004. Global Biogeochemical Cycles, 20, GB4017.

826 Tanhua, T., Körtzinger, A., Friis, K., Waugh, D.W., Wallace, D.W.R., 2007. An estimate of anthropogenic CO2 inventory from decadal changes in oceanic carbon content. Proceedings of the National Academy of Sciences, 104, 3037-3042.

829 Tanhua, T., Steinfeldt, R., Key, R.M., Brown, P., Gruber, N., Wanninkhof, R., Pérez, F., Körtzinger, A., Velo, A., Schuster, U., van Heuven, S., Bullister, J.L., Stendardo, I., Hoppema, M., Olsen, A., Kozyr, A., Pierrot, D., Schirnick, C., Wallace, D.W.R., 2010a. Atlantic Ocean CARINA data: overview and salinity adjustments. Earth system science data, 2, 17-34.

834 Tanhua, T., van Heuven, S., Key, R.M., Velo, A., Olsen, A., Schirnick, C., 2010b. Quality control procedures and methods of the CARINA database. Earth system science data, 2, 35-49.

837 Tanhua, T., Waugh, D.W., Wallace, D.W.R., 2008. Use of SF6 to estimate anthropogenic CO2 in the upper ocean. Journal of Geophysical Research C: Oceans, 113.

839 Thomas, H., Ittekkot, V., 2001. Determination of anthropogenic CO2 in the North Atlantic Ocean using water mass ages and CO2 equilibrium chemistry. Journal of Marine Systems, 27, 325-336.

842 Touratier, F., Azouzi, L., Goyet, C., 2007. CFC-11, Δ14C and 3H tracers as a means to assess anthropogenic CO2 concentrations in the ocean. Tellus, Series B: Chemical and Physical Meteorology, 59, 318-325.

845 Touratier, F., Goyet, C., 2004. Definition, properties, and Atlantic Ocean distribution of the new tracer TrOCA. Journal of Marine Systems, 46, 169-179.

847 Vázquez-Rodríguez, M., Padin, X.A., Pardo, P.C., Ríos, A.F., Pérez, F.F., 2012. The subsurface layer reference to calculate preformed alkalinity and air–sea CO2 disequilibrium in the Atlantic Ocean. Journal of Marine Systems, 94, 52-63.

Vázquez-Rodríguez, M., Touratier, F., Lo Monaco, C., Waugh, D.W., Padin, X.A., Bellerby, R.G.J., Goyet, C., Metzl, N., Ríos, A.F., Pérez, F.F., 2009a. Anthropogenic carbon distributions in the Atlantic Ocean: data-based estimates from the Arctic to the Antarctic. Biogeosciences, 6, 439-451.

Vázquez-Rodríguez, M., Padin, X.A., Ríos, A.F., Bellerby, R.G.J., Pérez, F.F., 2009b. An upgraded carbon-based method to estimate the anthropogenic fraction of dissolved CO2 in the Atlantic Ocean. Biogeosciences Discuss., 6, 4527.

Velo, A., Vázquez-Rodríguez, M., Padín, X.A., Gilcoto, M., Ríos, A.F., Pérez, F.F., 2010. A multiparametric method of interpolation using WOA05 applied to anthropogenic CO2 in the atlantic. Scientia Marina, 74, 21-32.

Wanninkhof, R., Park, G.-H., Takahashi, T., Feely, R.A., Bullister, J.L., Doney, S.C., 2013. Changes in deep-water CO2 concentrations over the last several decades determined from discrete pCO2measurements. Deep Sea Research Part I: Oceanographic Research Papers, 74, 48-63.

Watson, A.J., Nightingale, P.D., Cooper, D.J., 1995. Modelling atmosphere-ocean CO2 transfer. Philosophical Transactions - Royal Society of London, B, 348, 125-132.

Waugh, D.W., Haine, T.W.N., Hall, T.M., 2004. Transport times and anthropogenic carbon in the subpolar North Atlantic Ocean. Deep-Sea Research Part I: Oceanographic Research Papers, 51, 1475-1491.

Waugh, D.W., Hall, T.M., McNeil, B.I., Key, R., Matear, R.J., 2006. Anthropogenic CO2 in the oceans estimated using transit time distributions. Tellus, Series B: Chemical and Physical Meteorology, 58, 376-389.

Yool, A., Oschlies, A., Nurser, A.J.G., Gruber, N., 2010. A model-based assessment of the TrOCA approach for estimating anthropogenic carbon in the ocean. Biogeosciences, 7, 723-751.

Figure Legends

Figure 1. a) A05 section tracks for the 1992 (green), 1998 (red), 2004 (dark blue), 2010 (light blue) and 2011 (yellow) cruises. **b)** Regions, layers and defined boxes over the salinity distribution of the 2011 cruise. The sections were zonally divided into five regions: Region 0 (Florida Strait, 80°W to 78°W), region 1 (78°W to 70°W), region 2 (70°W to 45°W), region 3 (45°W to 30°W) and region 4 (30°W to 10°W). Six density layers were defined identifying the main water masses of the Subtropical North Atlantic: uNACW (σ_0<26.7 kg·m^{-3}), lNACW (26.7 kg·m^{-3}<σ_0<27.2 kg·m^{-3}), AAIW (27.2 kg·m^{-3}<σ_0<27.6 kg·m^{-3}), uNADW (σ_0>27.6 kg·m^{-3} and σ_2<37 kg·m^{-3}), lNADW (σ_2>37 kg·m^{-3} and σ_4<45.9 kg·m^{-3}) and AABW (σ_4>45.9 kg·m^{-3}).

Figure 2. Mean distributions of $C_{ant}^{\varphi C_T^0}$ (µmol·kg^{-1}) along the A05 section for the eastern (right panel) and western (left panel) subtropical North Atlantic basins, in 1992 (red line) and 2011 (blue line). The respective shaded areas correspond to the standard deviation of the mean $C_{ant}^{\varphi C_T^0}$ estimates.

Figure 3. Averaged C_{ant} concentrations (µmol·kg^{-1}) within each box and its uncertainty indicated by the coloured dots and the corresponding error bars (double of std): $[C_{ant}^{\varphi C_T^0}]$ (red), $[C_{ant}^{TrOCA}]$ (blue), $[C_{ant}^{\Delta C^*}]$ (green), $[C_{ant}^{TTD}]$ (grey). The associated coloured lines are the respective DT (µmol·kg^{-1}·yr^{-1}). Each horizontal panel corresponds to each layer, which are divided in subpanels identifying the regions. Mean TSSR ± standard deviation is indicated in each box as the area between purple dotted lines

Figure 4. C_{ant} storage rates (µmol·kg^{-1} yr^{-1}), with their uncertainty. The storage rates calculated trough the DT (coloured circles) or the TSSR (coloured crosses) approaches, by using each method: ΔC^* (green), φC_T^0 (red), TrOCA (blue) and TTD (grey). Mean values, considering the four methods, through the DT (pink) and the TSSR (purple) approaches are also shown. Each horizontal panel corresponds to each layer, which are divided in subpanels identifying the regions. The yellow dashed-dotted line indicates the average DT along each whole layer, summing up the regions. Vertical thicker lines

highlight the boundary between the Florida Strait and the main section and between the western and the eastern basins along the Mid-Atlantic Ridge. The corresponding values are reported in Table C1, in Appendix C

Table 1. Cruises information on the repeat section A05.

Cruise name (Expocode)	Dataset	Year	Period	Research Vessel	Sampled stations	CO_2 parameters[a]	Carbon related data PI(s)	Data adjustments in this study ($\mu mol \cdot kg^{-1}$)
29HE06_1-3	GLODAP	**1992**	7/14 -8/15	*R/V Bio Hespérides*	112	A_T(m), pH(m), C_T (calc)	F. Millero /A. Ríos	A_T(+4)[b] pH(-0.009 units)[b]
33RO19980123	CARINA	**1998**	1/23-2/24	*R/V Ronald H. Brown*	130	A_T(m), pH(m), C_T(m)	R. Wanninkhof/ R.Feely	O_2(*0.99)[c]
74DI20040404	CARINA own data	**2004**	4/4-5/10	*R/V Discovery*	125	A_T(m), C_T(m)	U. Schuster	SiO_4 (*0.98)[d] NO_3 (*0.97)[d]
74DI20100106	New data[e]	**2010**	1/6-2/18	*R/V Discovery*	135	A_T(m), C_T(m)	U. Schuster	O_2(*1.03)[f] SiO4 (*0.94)[f]
--	New data	**2011**	1/28-3/14	*R/V Sarmiento de Gamboa*	167	A_T(m), pH(m), C_T (calc)	E F. Guallart	--

[a] (m) = measured parameter, (calc) = calculated parameter.

[b](Guallart *et al.*, 2013)

[c](Stendardo *et al.*, 2009)

[d](Tanhua et al., 2010a)

[e](Schuster *et al.*, 2013)

Figure 1
Click here to download high resolution image

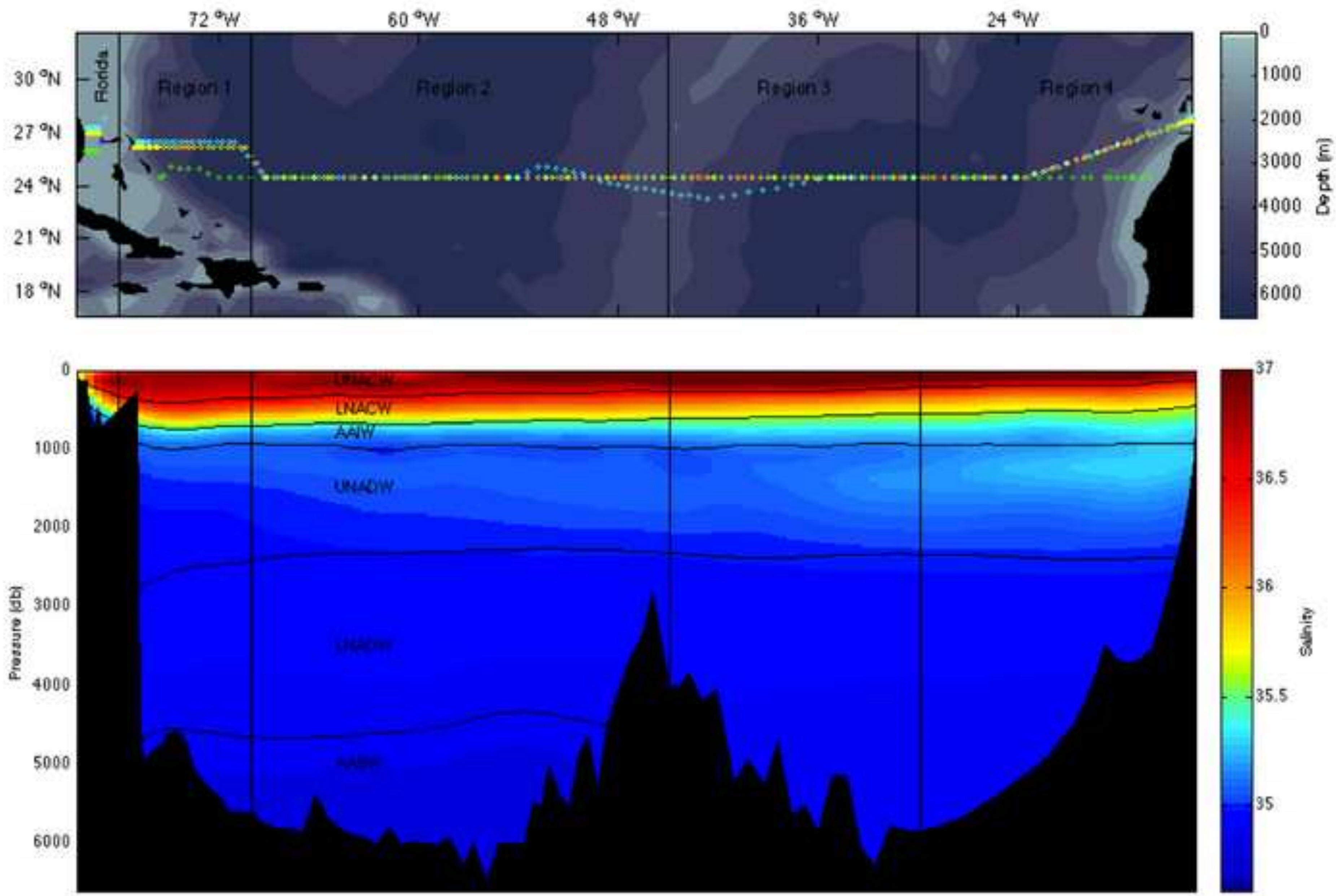

Figure 2
Click here to download high resolution image

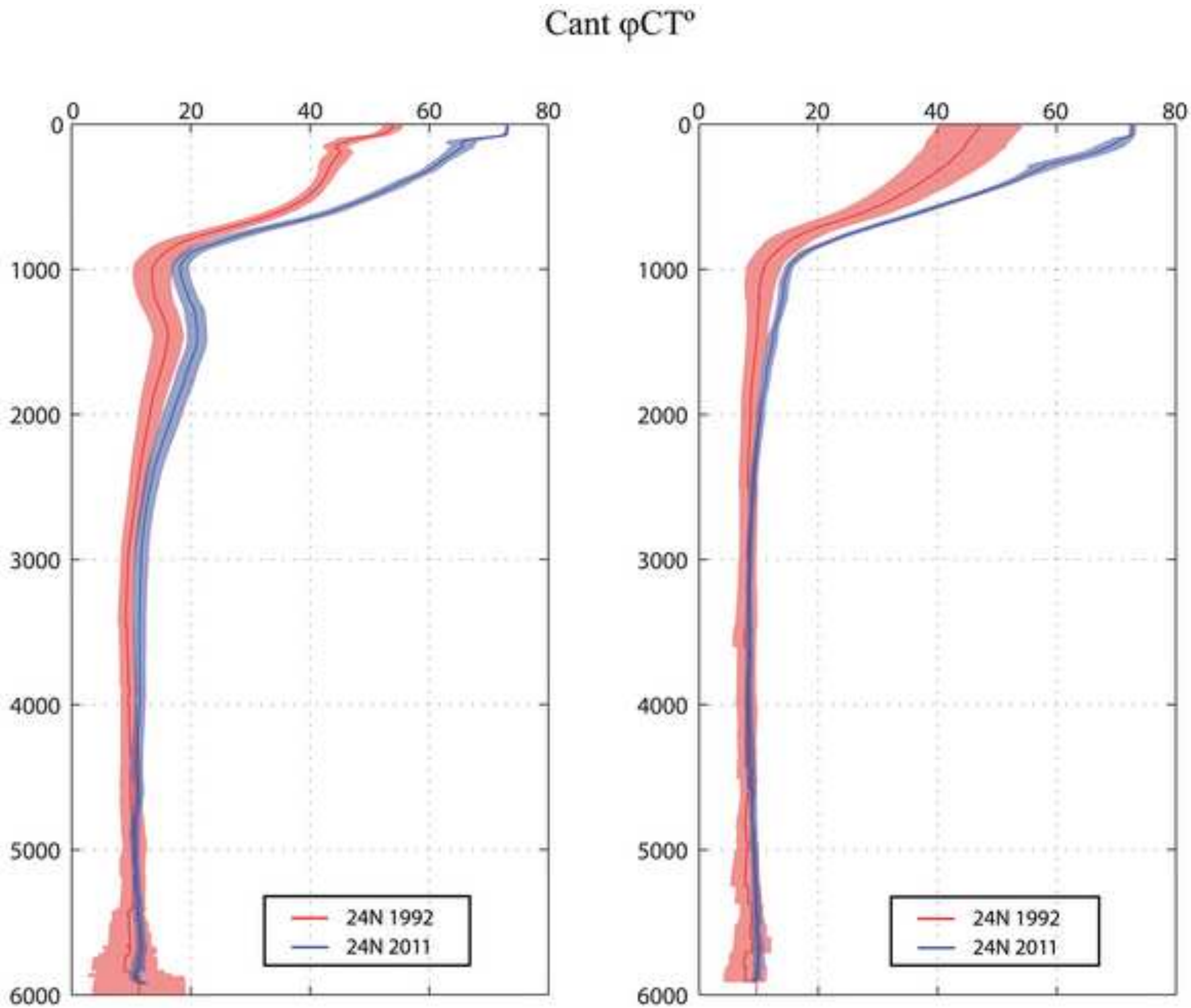

Figure 3

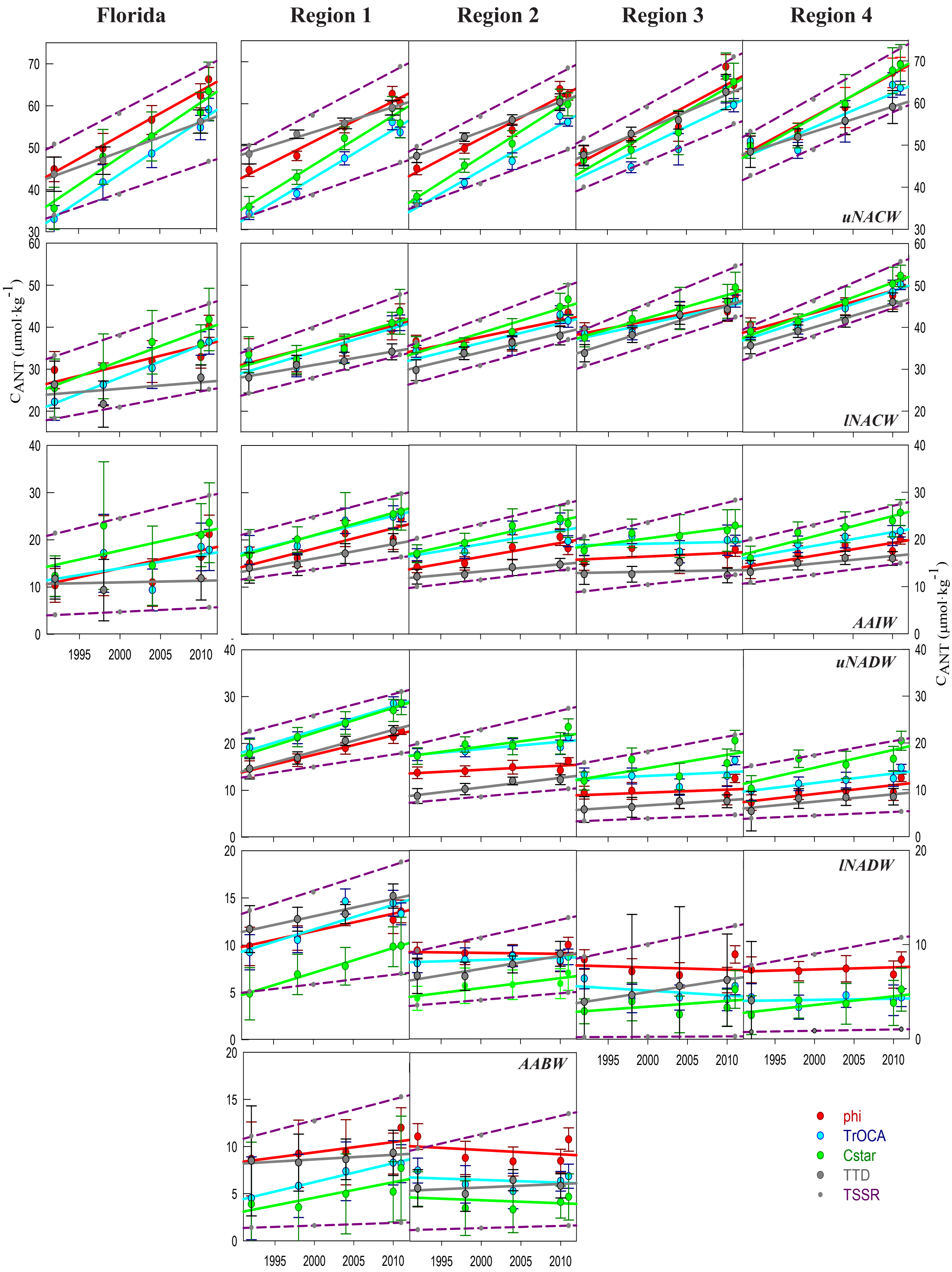
Florida
Region 1
Region 2
Region 3
Region 4
uNACW
lNACW
AAIW
uNADW
lNADW
AABW
CANT (µmol·kg-1)
1995
2000
2005
2010
phi
TrOCA
Cstar
TTD
TSSR

Figure 4

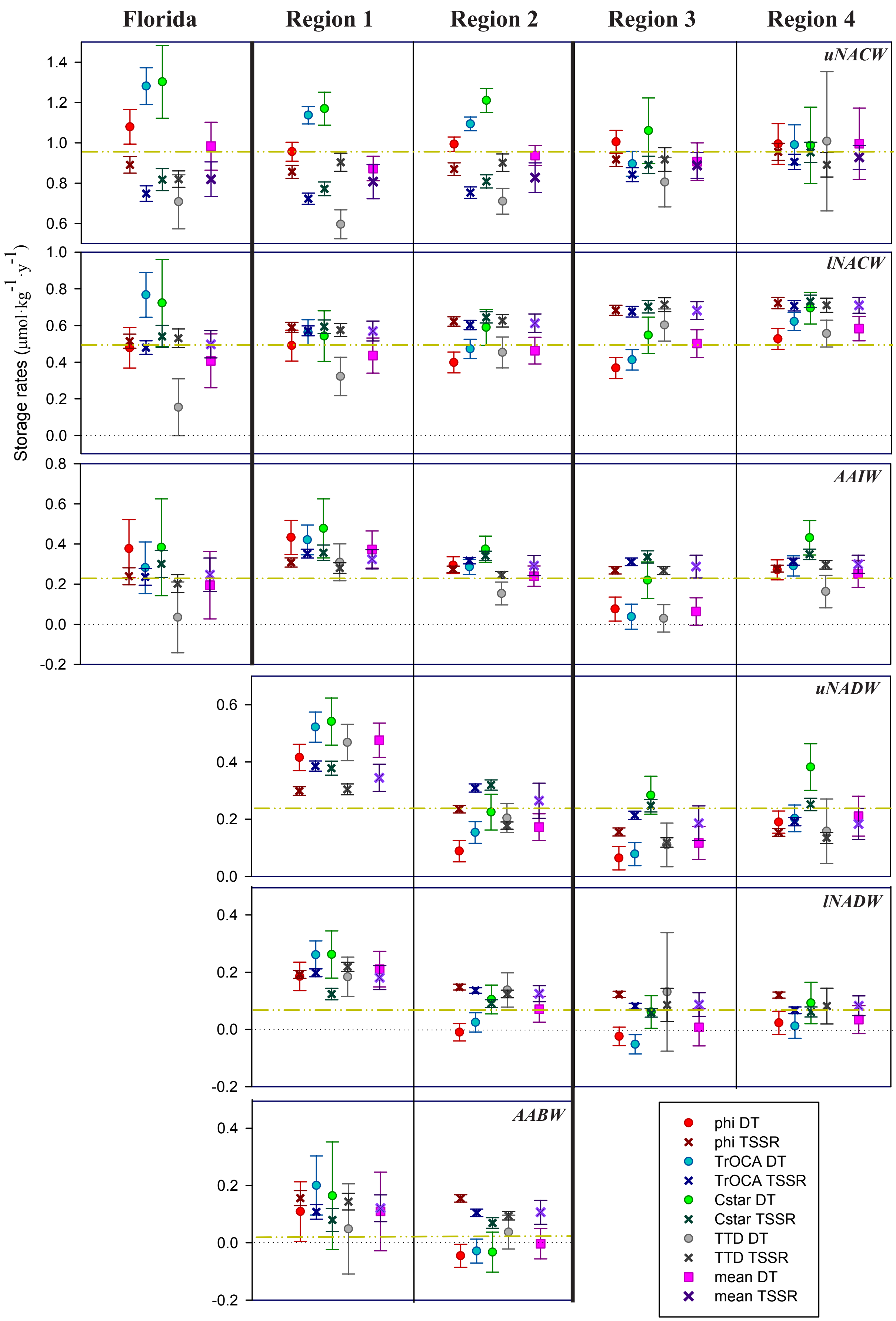
Florida
Region 1
Region 2
Region 3
Region 4
uNACW
lNACW
AAIW
uNADW
lNADW
AABW
Storage rates (μmol·kg⁻¹·y⁻¹)
phi DT
phi TSSR
TrOCA DT
TrOCA TSSR
Cstar DT
Cstar TSSR
TTD DT
TTD TSSR
mean DT
mean TSSR

Supplementary Captions

Click here to download e-component: E.F.Guallart_Supplementary_Captions.docx

Supplementary Information

Click here to download e-component: E.F.Guallart_Supplementary_Information.docx